THE JOURNAL OF PHYSICAL CHEMISTRY C

Article

pubs.acs.org/JPCC

# CO- and NO-Induced Disintegration and Redispersion of Three-Way Catalysts Rhodium, Palladium, and Platinum: An ab Initio Thermodynamics Study

Bryan R. Goldsmith,[†] Evan D. Sanderson,[‡] Runhai Ouyang,[#] and Wei-Xue Li*,[#]

[†]Department of Chemical Engineering, University of California, Santa Barbara, California 93106-5080, United States

[‡]Department of Chemistry and Biochemistry, University of California, Santa Barbara, California 93106-9510, United States

[#]State Key Laboratory of Catalysis, Dalian Institute of Chemical Physics, Chinese Academy of Sciences, Dalian 116023, China

Supporting Information

**ABSTRACT:** Disintegration of supported nanoparticles (NPs) in the presence of reactants can lead to catalyst deactivation or be exploited to redisperse sintered catalysts. To better understand the stability of $TiO_2$(110)-supported three-way catalysts Rh, Pd, and Pt NPs during $NO_x$ and CO reduction, we present an ab initio thermodynamics study of the feasibility for these NPs to disintegrate into adatom-reactant complexes across a large parameter space of temperatures, pressures, and sizes. The tendencies for disintegration and redispersion between supported Rh, Pd, and Pt NPs are established. Compared to both Pd and Pt, Rh NPs are found to be more susceptible to either NO- or CO-induced disintegration, due to the large and exothermic formation energy of the Rh adatom complexes. Moreover, NO is a more efficient reactant for particle redispersion than CO. These findings provide valuable insights for how to either prevent reactant-induced NP disintegration or facilitate reactant-induced redispersion of sintered catalysts.

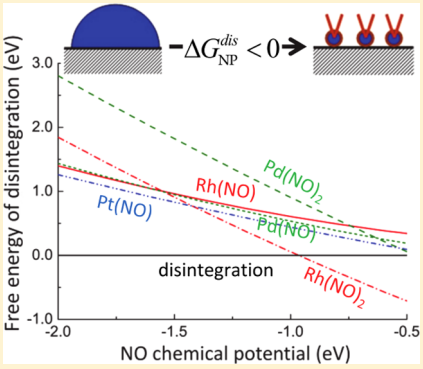


## 1. INTRODUCTION

Stricter vehicle emission control standards require the use of efficient $NO_x$ and CO oxidation catalysts to reduce toxic exhaust emissions. Typically, dispersed precious metal nanoparticles (NPs) such as Rh, Pd, and Pt supported on oxides are the primary components of automotive three-way-catalyst devices.[1−3] Because rare and costly metals are used in these devices, increasing the catalyst's lifetime and recyclability is extremely important. Furthermore, it is imperative to control and optimize NP size during catalytic applications since it can strongly influence catalytic activity[4−7] and stability.[7−10] It was believed that the increased activity of NPs, compared to their bulk counterpart, comes from the presence of a high amount of coordinatively unsaturated sites,[5,7,11] additional active sites at the metal/support boundaries,[12−14] or even quantum size effects.[7,15,16]

A long-standing problem is that the NP size distribution can change under operating conditions due to phenomena such as sintering[17−22] or disintegration,[8,23−29] which can deactivate the catalyst. Elevated temperatures and/or the presence of gas species can promote even further the growth of NPs at the expense of smaller ones.[9,20,30] Further complicating matters is that supported NPs can undergo a dynamic interplay between ripening and disintegration.[25,27,28,31,32] For example, the sintering and subsequent redispersion of supported Pd NPs during CO/NO cycling has been reported.[25,27] Nevertheless, it is imperative to have an understanding of the ripening and the disintegration processes so strategies can be developed to enhance control of the NP size distribution.

Though it is well-documented in literature that the presence of reactants could accelerate the ripening of supported NPs, the precise role of reactants is challenging to quantify experimentally. However, steady progress has been made in experimentally identifying reactant-induced ripening mechanisms. Recently, Parkinson et al. reported CO-induced sintering of Pd adatoms supported on $Fe_3O_4$(001), and that Pd-carbonyl species were responsible for the observed increase in surface mobility.[22] A 500 times increase of Pt adatom self-diffusion in the presence of hydrogen due to the formation of mobile Pt−hydrogen complexes[33] and CO-induced Smoluchowski ripening of Pt clusters on graphene/Ir(111) have also been observed.[34]

Numerous experimental studies have reported the reactant-induced disintegration of supported metal NPs, e.g., Rh,[23,26,35,36] Pd,[25,27] and Pt,[28,37−41] among others.[42−45] Reactant-induced disintegration of metal NPs into adatom complexes occurs when the metal−reactant bonding overcomes the metal−support and interatomic metal−metal interactions. Using reactants to redisperse already sintered particles is a viable strategy to recover lost catalytic activity.[44−48] For instance, redispersion of $TiO_2$-supported Au clusters by $CH_3I$

**Received:** March 4, 2014
**Revised:** April 14, 2014
**Published:** April 16, 2014

   dx.doi.org/10.1021/jp502201f | J. Phys. Chem. C 2014, 118, 9588−9597

was found to increase catalytic activity toward ethanol dehydration.[44] On the other hand, sometimes it is desirable to prevent reactant-induced disintegration, e.g., the disintegration of $SiO_2$-supported Rh NPs into carbonyl hydride (Rh(CO)H) adatom complexes during propionaldehyde formation was reported to reduce catalyst activity.[49] Though the formation and stability of adatom complexes was found to depend strongly on NP size, temperature, and gas pressure,[23,25,27,28] it is difficult to quantify the individual contributions experimentally. Furthermore, it still remains a challenge to efficiently prevent catalyst deactivation from reactant-induced disintegration or to systematically redisperse sintered catalysts.

Recently, we developed an ab initio atomistic thermodynamic theory that could describe quantitatively the sintering and disintegration of supported NPs under reaction conditions.[50] In this work, the tendency to form the metal−reactant complexes, which depends sensitively on the reactant−metal−support interaction, NP size, as well as the temperature and reactant pressure, was formulated and quantified to understand the reactant-assisted ripening and induced disintegration. We proposed that to suppress the sintering and/or prevent the disintegration induced by reactants, it was important to find a support that could prevent the formation of the metal−reactant complexes. In contrast, to facilitate catalyst disintegration for redispersion of sintered catalysts on a given support, it was needed to find a reactant that could bind strongly to the supported metal adatoms and form stable adatom-reactant complexes. The theory, which makes use of ab initio thermodynamics,[51−54] was justified by application to $TiO_2$(110)-supported Rh NPs in a CO environment, and extraordinary agreement with experiment over wide ranges of temperature, pressure, and particle size was obtained.

To help improve the stability and recyclability of precious three-way catalysts during $NO_x$ and CO reduction, here we apply the aforementioned theory to discern the impact of NO and CO on $TiO_2$(110)-supported Pt, Pd, and Rh NP stability and disintegration. We will particularly address the following questions: among supported Rh, Pd, and Pt catalysts, which one is more susceptible to disintegration; second, among NO and CO, which one is more efficient for the redispersion of the low surface area catalyst; finally, how sensitive do these results depend on the particle size, temperature, and partial pressure. To address these goals, formation energies of Pt, Pd, and Rh adatoms and adatom complexes were computed as well as the influence of CO and NO binding on NP surface energies. The impact of varying CO and NO chemical potential and NP size on supported NP energetics was examined over a large parameter space, and equilibrium thermodynamic predictions of Pt, Pd, and Rh NP disintegration via formation of adatom complexes were put forward. The insights revealed are expected to have general implications for strategies to either prevent catalyst disintegration or facilitate catalyst redispersion.

## 2. GIBBS FREE ENERGY OF REACTANT-INDUCED PARTICLE DISINTEGRATION

The procedure used to describe supported metal particle energetics and their corresponding Gibbs free energy of particle disintegration under reaction conditions is discussed here briefly, and a complete description can be found in our previous work by Ouyang et al.[50]

The feasibility of reactant-induced NP disintegration to occur under a given set of reaction conditions can be predicted by using the Gibbs free energy of disintegration $\Delta G_{NP}^{dis}$. This equilibrium thermodynamic expression describes whether a supported particle with radius of curvature $R$ will disintegrate completely into isolated adatom complexes (depicted in Figure 1):

$$\Delta G_{NP}^{dis}(R, T, P_X) = E^f_X - \Delta\bar{E}_{NP}(R) - n\Delta\mu_X(T, P_X) - T\Delta S \quad (1)$$

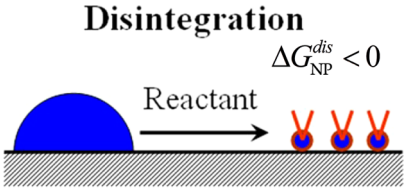


**Figure 1.** Reactant-induced disintegration of metal particles into adatom complexes occurs when the metal−reactant bonding is greater than the metal−support and interatomic metal−metal interactions. This phenomenon can be expected to occur when the Gibbs free energy of disintegration $\Delta G_{NP}^{dis}$ is negative.

where $E^f_X$ is the formation energy of an isolated adatom complex on the support with respect to the bulk metal and the reactants in the gas phase, $\Delta\bar{E}_{NP}$ is the average energy per atom of a metal particle with respect to the bulk metal in the presence of reactants, $n$ is the number of gas molecules bound to the adatom complex, $\Delta\mu_X(T,P_X)$ is the gas phase chemical potential, and $\Delta S$ is the configurational entropy of the adatom complexes on the support (see the Supporting Information for the configurational entropy formula used).[50] Here translational entropy is neglected, so eq 1 should be limited to instances where the adatom complexes are bound strongly to the support.

If $\Delta G_{NP}^{dis}$ is negative, then the NP should be expected to disintegrate under equilibrium conditions. From eq 1, it is predicted that an exothermic adatom complex formation energy and a small particle radius (and a corresponding increase in surface energy) will promote NP disintegration. The gain in configurational entropy due to adatom complex formation is offset by the loss of entropy for gas molecules binding to the adatom. Increasing the reactant species chemical potential, $\Delta\mu_X(T,P_X)$, by raising pressure or lowering temperature (although not too low as to kinetically hinder disintegration) will also enhance the thermodynamic driving force for NP disintegration. All quantities in eq 1 can be obtained by first-principles calculations.[50] This allows the rapid calculation of the effects of reactant partial pressure, temperature, NP size, as well as particle morphology on the stability of supported NPs toward disintegration into adatom complexes.

## 3. COMPUTATIONAL METHODOLOGY

Spin-polarized density functional theory calculations were performed by using the Vienna Ab-initio Simulation Package (VASP 5.2.12).[55−57] The Kohn−Sham wave functions were expanded by plane waves with a kinetic energy cutoff of 400 eV. The interactions between valence electrons and ions were described by using the projected augmented wave method.[58] The Revised Perdew−Burke−Erzernhof (RPBE) functional was used for all calculations.[59] Rutile $TiO_2$(110) ($a$ = $b$ = 4.70 Å and $c$ = 2.96 Å) was modeled by a four trilayer slab with periodicity (4 × 2) separated by a 15 Å vacuum layer, which has


dx.doi.org/10.1021/jp502201f | J. Phys. Chem. C 2014, 118, 9588−9597

been shown to be well-converged in size.[60] The atoms in the top two trilayers were unconstrained and the atoms in the bottom two trilayers were constrained in their bulk-truncated positions. All systems were relaxed by using the conjugate-gradient algorithm until the Hellman−Feynman force[61] on each atom was less than 0.03 eV/Å. The Γ point was used to sample the surface Brillouin zone, as has been done in previous studies involving $TiO_2$(110).[62,63] Because we are only looking for qualitative trends in our study, and the typical density functional error on adsorption energies can be upward of ±0.1 eV, the chosen force convergence and Brillouin zone sampling criteria was deemed sufficient.

Particle surface energies of Pt, Pd, and Rh were approximated as the surface energies of Pt(111), Pd(111), and Rh(111) (1 × 1) slab models, which were converged to 1 meV/Å$^2$ with respect to the thickness of the slab. At equilibrium, the (111) facets of Pt, Pd, and Rh NPs contribute the most to the total surface energy.[64] It has been shown previously that the Rh(111) surface energy closely approximates the average surface energy of an infinite size Wulff constructed NP.[50] Computed surface energetics of the (111) facets ($A$ = 6.452 Å$^2$) were 0.113, 0.086, and 0.093 eV/Å$^2$, for Rh, Pd and Pt, respectively, which are in close agreement with a previous computational report, albeit upward of a 30% underprediction compared to experiments for Pd and Pt.[64] The underestimation of the computed surface energies will translate into roughly a 0.1 eV overprediction (too positive) of the computed disintegration free energies compared to if experimental surface energies were used. (4 × 4) slabs were used when modeling surface coverage effects of CO and NO adsorption on the particle surface energies. Bulk lattice constants of Rh, Pd, and Pt were computed to be 3.86, 3.95, and 3.98 Å, respectively, which are all within 2% of experimental measurements.[65] The molar volumes Ω of Rh, Pd, and Pt were computed to be 14.39, 15.42, and 15.77 Å$^3$.

## 4. RESULTS AND DISCUSSION

**4.1. Formation of Metal Adatoms and Adatom Complexes.** Computed formation energies of supported metal adatoms $E^f_{ma}$ and adatom complexes $E^f_X$ (with respect to the bulk counterpart), where the bound reactant species X are either CO or NO, are reported in Table 1. A number of adatom adsorption geometries were computed, and only the most stable adatom positions found were reported and used to compute $E^f_{ma}$. The corresponding most stable adatom adsorption geometries are presented in Figure S1 in the Supporting Information. In agreement with previous reports, we find that at low coverages the Pd adatom prefers a 2-fold coordinated O site[66] and that the Rh adatom prefers a hollow site coordinated with a bridging oxygen and a 5-fold Ti.[50] The Pt adatom was computed to prefer the hollow site on clean $TiO_2$(110). All computed adatom formation energies are endothermic, with the Pt and Rh adatom $E^f_{ma}$ being 1.11 and 0.87 eV larger than the Pd adatom $E^f_{ma}$ (2.01 eV), respectively. The endothermic formation energies suggest that a low concentration of metal adatoms will be present on the support under vacuum conditions.

**Table 1. Formation Energies (eV) of $TiO_2$(110)-Supported Metal Adatoms $E^f_{ma}$ and Mono- and Di-adatom Complexes $E^f_X$, Where X = CO or NO, As Well As the Binding Energies of the Adatom Complexes to the Support $E^b_X$**

| metal species | Rh | Pd | Pt |
|---|---|---|---|
| $E^f_{ma}$ | 2.88 | 2.01 | 3.12 |
| $E^f_{CO}$(mono) | 0.75 | 0.26 | 0.09 |
| $E^f_{CO}$(di) | −1.35 | −0.54 | −0.69 |
| $E^f_{NO}$(mono) | −0.02 | −0.05 | −0.10 |
| $E^f_{NO}$(di) | −1.58 | −0.67 | −0.68 |
| $E^b_{CO}$(mono) | −1.74 | −0.62 | −1.41 |
| $E^b_{CO}$(di) | −2.62 | −0.08 | −0.07 |
| $E^b_{NO}$(mono) | −1.72 | −1.44 | −2.61 |
| $E^b_{NO}$(di) | −3.05 | −0.71 | −0.05 |

In this study, we consider either one or two molecules of NO or CO in each adatom complex, as higher coordinated complexes were computed to prefer the gas phase. Since we do not consider gas phase disintegration in this study, we neglect all adatom complexes with a CO or NO coordination greater than two. The corresponding formation energies of the mono- or di-adatom complexes $E^f_X$ are presented in Table 1. A variety of adatom complex geometries were tested, and only the most stable adsorption configurations were reported and used to compute $E^f_X$. The most relevant adatom complex geometries are shown in Figures S2−S4 in the Supporting Information. For each metal, the adatom-monocarbonyl formation energy $E^f_{CO}$(mono) was computed to be endothermic. On the other hand, the adatom-mononitrosyl formation energy $E^f_{NO}$(mono) was computed to be slightly exothermic for each metal, indicating stronger adatom stabilization due to NO binding than CO binding. For all considered metals, the formation energy of the adatom-dicarbonyl $E^f_{CO}$(di) is calculated to be more favorable and exothermic than $E^f_{CO}$(mono). Similarly, for each metal the formation energy of the adatom-dinitrosyl $E^f_{NO}$(di) is found to be more favorable and exothermic than its respective $E^f_{NO}$(mono).

The formation energy of the Rh adatom complex is more sensitive to increases in coordination number than both the Pt and the Pd adatom complexes. For example, $E^f_{CO}$(mono) = 0.75 and $E^f_{CO}$(di) = −1.35 eV for Rh (over a two electronvolt stabilization in electronic energy), while the Pd and the Pt adatom complex formation energies become more exothermic by about 0.8 eV upon binding of a second CO molecule. A similar trend is observed upon comparing the formation energy differences between $E^f_{NO}$(mono) and $E^f_{NO}$(di) for each metal, i.e., the Rh adatom is more sensitive to additional NO binding than either the Pd or the Pt adatom. This electronic effect can be rationalized by noticing that Rh is less noble than Pd or Pt, and therefore is more responsive to the additional electron density from either CO or NO.

To quantify how strong the adatom complexes interact with the support, the binding energy, $E^b_X$ was computed

$$E^b_X = E_{mc/ox} - E_{mc} - E_{ox} \quad (2)$$

where $E_{mc/ox}$ is the total energy of the adatom complex on the support, $E_{mc}$ is the total energy of the adatom complex in the gas phase (which was constrained to its adsorbed structure), and $E_{ox}$ is the total energy of the support. Binding energies are in Table 1 for the adatom-carbonyl and the adatom-nitrosyl complexes. The Rh adatom-monocarbonyl, Rh(CO) and the Rh adatom-mononitrosyl, Rh(NO) are computed to interact strongly with the support, both having binding energies of about −1.7 eV. The binding energies of the Rh adatom-dicarbonyl, $Rh(CO)_2$ and the Rh adatom-dinitrosyl, $Rh(NO)_2$ to the $TiO_2$(110) support are even more exothermic than the


dx.doi.org/10.1021/jp502201f | J. Phys. Chem. C 2014, 118, 9588−9597

Rh(CO) and the Rh(NO) complexes. The $Pd(CO)_x$ and the $Pd(NO)_x$ complexes were computed to bind less strongly to the support than the respective $Rh(CO)_x$ and $Rh(NO)_x$ complexes, which should result in a heightened mobility on the support for the Pd adatom complexes compared to the Rh adatom complexes.

The Pt(CO) and the Pt(NO) binding energies are more exothermic than the Pd(CO) and the Pd(NO) complexes by −0.79 and −1.17 eV, respectively, while the $Pt(CO)_2$ and the $Pt(NO)_2$ complexes are predicted to have a negligible binding to the support (−0.07 and −0.05 eV, respectively), and thus are considered to be in the gas phase. As predicted, experimental observations suggest that $Pt(CO)_x$ complexes are less stable on $TiO_2(110)$ than $Rh(CO)_x$ complexes,[41] and that ultimately gas phase Ostwald Ripening will occur for disintegrated Pt NPs but not for Rh NPs.[28] Likewise, the $Pd(CO)_2$ complex is computed to bind very weakly to the support, −0.08 eV, and is also considered to be in the gas phase (see Figure S4 in the Supporting Information).

It is well-known that NP disintegration in the presence of an oxygen environment can occur in the gas phase via the formation of volatile oxides,[9,29,67−69] so a complete account of disintegration mechanisms should consider these possible pathways. In this study, however, we will focus on disintegration by the formation of adatom complexes bound strongly to the support, and therefore will not consider the $Pd(CO)_2$, $Pt(CO)_2$, and $Pt(NO)_2$ complexes, as well as higher order complexes, in the disintegration analysis.

**4.2. CO or NO Adsorption on Pt, Pd, or Rh NPs.** The (111) surface energy of Pt, Pd, and Rh, being the most abundant exposed facet for each metal, is used as an approximation of the average surface energy for each metal particle.[50,70] The (111) surfaces of Pt, Pd, and Rh were subsequently used to model NO and CO coverage effects on the NP surface energetics. This approximation implicitly assumes size-independent adsorption energies[71,72] and surface energies.[73] The assumption of size-independent metal surface energies will be tested later in this section.

We follow previous literature reports for choosing CO and NO adsorption configurations on the (111) surfaces. The chosen adsorption configurations of CO on Pt(111) and Pd(111) were based on a report using a combined density functional theory and lattice gas Monte Carlo approach.[74] CO adsorption positions on Rh(111) were based on our previous computational report that used experimental evidence to justify the use of chosen adsorption positions as a function coverage.[50] NO coverage dependent adsorption configurations on Pt(111), Pd(111), and Rh(111) were used as computationally predicted by Zeng et al.[75] (see Figures S5−S10 in the Supporting Information for the adsorption configurations used).

Average binding energies as a function of surface coverage for CO, $E_{CO}^{ad}(\theta_i)$ and NO, $E_{NO}^{ad}(\theta_i)$ for each metal are given in Table S1 of the Supporting Information. In agreement with a previous report, CO was found to bind more strongly to Pt(111) than Pd(111) at high coverages due to reduced lateral interactions.[74] Additionally, it was computed that at low coverages CO prefers either the HCP or FCC site on Pd(111),[76] while NO prefers the FCC site on Pd(111).[75,77] Similarly, NO was computed to prefer the FCC site on Pt(111).[75,78] The average binding energy of CO is more exothermic on Rh(111) compared to Pt(111) and Pd(111) for all surface coverages. Interestingly, the average binding energy of NO is computed to be more exothermic than CO for all surface coverages on Rh(111) and Pd(111). Conversely, NO binds more strongly than CO to Pt(111) at intermediate coverages, while at higher coverages NO binds about 0.15 eV less strongly than CO. Strikingly, a significantly more exothermic NO adsorption energy on Rh(111) compared to Pd(111) and Pt(111) (between 0.3 and 0.6 eV) was computed, which will ultimately manifest itself in much higher coverages of NO on Rh NPs than for Pt or Pd NPs at a specified gas phase chemical potential. Perhaps most importantly, these general trends of the comparative adsorption energies between CO and NO on the metal surfaces are also observed for the stabilization of the adatoms due to reactant adsorption as recorded in Table 1, i.e., NO generally binds more strongly than CO to all the metal adatoms, and CO and NO both interact more strongly with the Rh adatoms compared to the Pt and the Pd adatoms.

At a given $T$ and $P_X$, the dynamic equilibrium between the NP surface and the gas phase is obtained when the corresponding differential binding energy of the adsorbates, which itself is a function of surface coverage, is equal to the gas phase chemical potential $\Delta\mu_X(T,P_X)$

$$E_X^{dif}(\theta_i) = \frac{d[\theta_i E_X^{ad}(\theta_i)]}{d\theta_i} = \Delta\mu_X(T, P_X) \quad (3)$$

Accordingly, both the coverage of adsorbates at a given $T$ and $P_X$ and the corresponding reduction in NP surface energy $\Delta\gamma_{me}$ can be determined. Quadratic fits for the CO and NO coverage dependent adsorption and differential binding energies on Pt(111), Pd(111), and Rh(111) are in Figure S11 of the Supporting Information.

Figures 2 and 3 show the NP surface energy reduction due to adsorption of CO and NO, respectively. The reduction of the

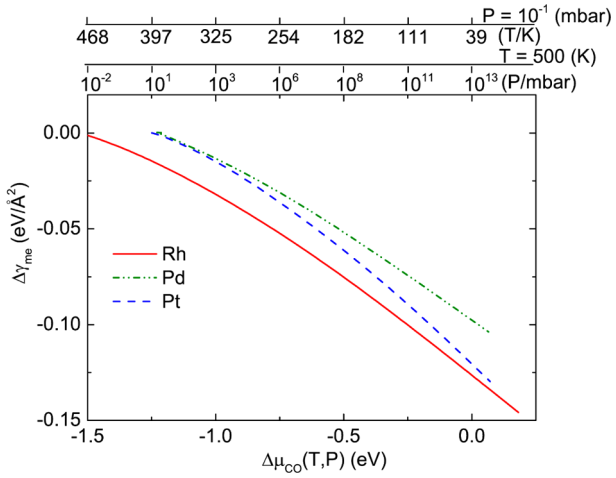


**Figure 2.** Reduction of surface energy $\Delta\gamma_{me}$ of Rh(111), Pd(111), and Pt(111) due to CO adsorption. The fitted quadratic polynomials to $\Delta\gamma_{me}$ for each metal are $\Delta\gamma_{me}^{Rh} = -0.0269\Delta\mu_{CO}^2 - 0.1263\Delta\mu_{CO} - 0.1298$, $\Delta\gamma_{me}^{Pd} = -0.024\Delta\mu_{CO}^2 - 0.1084\Delta\mu_{CO} - 0.0954$, and $\Delta\gamma_{me}^{Pt} = -0.047\Delta\mu_{CO}^2 - 0.1600\Delta\mu_{CO} - 0.1258$. Temperatures and pressures corresponding to the specified gas phase chemical potential are shown as the top axis.

Rh NP surface energy is larger than the reduction of the Pd and the Pt NP surface energy over a wide range of CO and NO chemical potentials due to stronger binding of the adsorbates. At 300 K and 0.1 mbar, typical applied conditions,[23] the corresponding gas phase chemical potentials of CO and NO are about −0.82 and −0.89 eV, respectively.[79] At the aforemen-


dx.doi.org/10.1021/jp502201f | J. Phys. Chem. C 2014, 118, 9588−9597

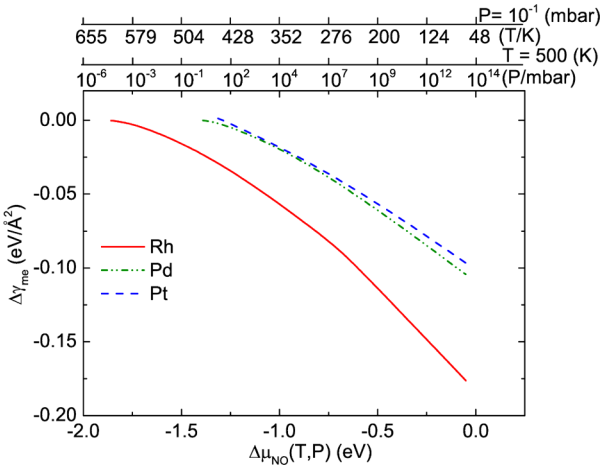


**Figure 3.** Reduction of surface energy $\Delta\gamma_{me}$ of Rh(111), Pd(111), and Pt(111) due to NO adsorption. The fitted quadratic polynomials to $\Delta\gamma_{me}$ for each metal are $\Delta\gamma_{me}^{Rh} = -0.0451\Delta\mu_{NO}^2 - 0.1913\Delta\mu_{NO} - 0.1994$, $\Delta\gamma_{me}^{Pd} = -0.0344\Delta\mu_{NO}^2 - 0.1279\Delta\mu_{NO} - 0.1109$, and $\Delta\gamma_{me}^{Pt} = -0.019\Delta\mu_{NO}^2 - 0.1018\Delta\mu_{NO} - 0.0985$. Temperatures and pressures corresponding to the specified gas phase chemical potential are shown as the top axis.

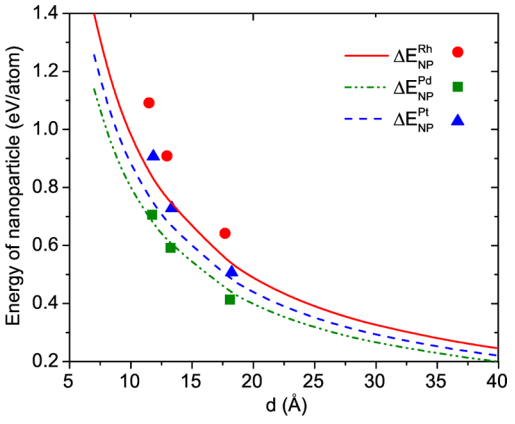


**Figure 4.** Average energy per atom $\Delta E_{NP}$ of Rh, Pt, and Pd NPs under vacuum vs particle diameter, $d$. The lines are predicted $\Delta E_{NP} = 3\Omega\gamma_{me}/R$ (using a constant surface energy $\gamma_{me}$) and the points are the computed $\Delta E_{NP}$ based on the Wulff constructed NPs.

tioned $\Delta\mu_{CO}$, the surface energy reduction of Rh NP, $\Delta\gamma_{me}^{Rh}$ is about 0.03 eV/Å$^2$ lower compared to$\Delta\gamma_{me}^{Pd}$ or $\Delta\gamma_{me}^{Pt}$.

Qualitatively comparing between Figures 2 and 3, the surface energy stabilization from NO binding is greater than CO binding for the Rh NP at a given chemical potential, while for the Pt and the Pd NPs the trends behave similarly. The onset of CO adsorption to the NP surface, where $\Delta\gamma_{me}$ first becomes nonzero, is predicted to occur first for Rh, followed by Pt and Pd. On the other hand, the onset of NO adsorption is expected to occur first for Rh, and then Pd and Pt.

To test the approximation of using a size independent surface energy when modeling NPs, the average energy per atom of Wulff constructed NPs is computed and compared against constant surface energy predictions by using $\Delta E_{NP} = 3\Omega\gamma_{me}/R$.[50] The NPs were Wulff constructed[80] based on their (110)/(111) surface energy ratio (1.38, 1.04, and 1.27 for Rh, Pd, and Pt, respectively). The Wulff constructed NPs contained 55, 79, or 201 atoms and the radii used in eq 1 were computed as $R = (3N\Omega/4\pi)^{1/3}$ (see Figure S12 in the Supporting Information), where $N$ is the number of atoms.

In Figure 4, the predicted $\Delta E_{NP}$ using constant surface energies and the computed $\Delta E_{NP}$ based on Wulff construction are shown as lines and solid points, respectively. The $\Delta E_{NP}^{Rh}$ for Rh is based on a previous report by Ouyang et al.[50] For particle diameters ($d = 2R$) around 18 Å, using a constant surface energy to predict $\Delta E_{NP}$ yields good agreement with the computed values for Pt and Pd NPs based on Wulff construction, having deviations smaller than 0.03 eV/atom. However, differences between the two approaches up to 0.08 eV/atom are already found for the Rh NP at $d$ = 17.7 Å. These deviations are expected to become greater as NP size further decreases.[73] At diameters near 12 Å, the $\Delta E_{NP}$ predictions underestimate the computed values based on Wulff construction for both Rh and Pt, having differences up to 0.2 eV/atom for the Rh NP. However, for the small sizes, the predicted values agree surprisingly well with the computed values based on Wulff construction for the Pd and Pt NPs. For the Rh NP, the greater difference stems from the intrinsically higher surface energy of Rh compared to Pt and Pd. Nonetheless, the modest size effects on surface energy lead us to believe it is an acceptable approximation to use size independent surface energies when searching for qualitative trends in NP stability against disintegration, although for accurate barrier predictions for use in modeling sintering kinetics these size effects likely should be included.[73]

**4.3. Reactant Environment and Particle Size Effects on Supported NP Energetics.** The structure of a supported NP is determined by its thermodynamics and kinetics as well as the reaction conditions. Particle diameter and reaction environment play a critical role in determining NP surface energetics, and ultimately help govern supported NP stability against sintering or disintegration. In this section, the Rh, Pd, and Pt NP energetics for many particle diameters and under various NO and CO gas phase chemical potentials are examined. However, before proceeding further, we first note that experimentally the particle size is often measured by using the projected particle diameter $d = 2R\sin(\alpha)$, where $\alpha$ is the supported particle contact angle. In order to make better comparison to experiments, we use an estimated contact angle of $\pi/3$ for Rh, Pd, Pt NPs on $TiO_2(111)$,[23] which gives a radius of curvature $R = d/\sqrt{3}$. This radius based on the projected diameter is used in all of the following calculations.

The average energy per atom of a supported NP in the presence of reactants $\Delta\bar{E}_{NP}$ can vary greatly for different particle sizes and reaction conditions.[50] Contour lines of $\Delta\bar{E}_{NP}$ as a function of chemical potential and particle diameter for Rh, Pd, and Pt NPs are shown in the presence of CO (Figure 5) or NO (Figure 6). For a specified gas phase chemical potential, $\Delta\bar{E}_{NP}$ is computed to increase linearly vs $1/d$. At a given particle diameter, the particle becomes more stable ($\Delta\bar{E}_{NP}$ decreases) as the chemical potential of CO or NO becomes more positive. At less negative (alternatively higher) gas phase chemical potentials the surface coverage of reactant species will be higher, which stabilizes the NP through a reduction of its surface energy.

In Figures 5 and 6, it is observed that NPs with large diameters and a low chemical potential can acquire the same $\Delta\bar{E}_{NP}$ as smaller NPs but with a higher chemical potential. This implies a degeneracy of NP energetics over a broad range of particle sizes and reaction conditions, which is a consequence of reactant-induced stabilization and size-dependent particle energetics. Under a CO environment, for a given particle


dx.doi.org/10.1021/jp502201f | J. Phys. Chem. C 2014, 118, 9588−9597

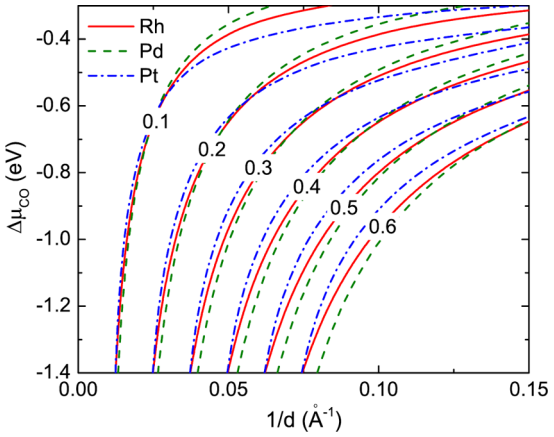


**Figure 5.** Effect of CO chemical potential and projected particle diameter on the average energy per atom of a supported Rh, Pd, or Pt NP ($\Delta\bar{E}_{NP}$ contours in eV).

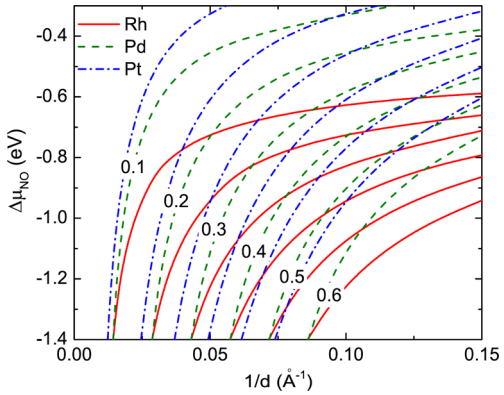


**Figure 6.** Effect of NO chemical potential and projected particle diameter on the average energy per atom of a supported Rh, Pd, or Pt NP ($\Delta\bar{E}_{NP}$ contours in eV).

diameter, Pd, Pt, and Rh NPs are computed to have a comparable $\Delta\bar{E}_{NP}$, typically differing by less than $\Delta\mu_{CO} = 0.05$ eV. On the contrary, the variation of $\Delta\bar{E}_{NP}$ under an NO environment is much greater between each supported metal particle. For instance, for Rh NPs of $1/d = 0.05$ Å$^{-1}$ in the presence of NO, $\Delta\mu_{NO} = -1.18$ eV gives $\Delta\bar{E}^{Rh}_{NP} = 0.3$ eV/atom, while $\Delta\mu_{NO} = -1.03$ and a $\Delta\mu_{NO} = -0.89$ eV are needed for the Pd and the Pt NPs, respectively, to yield the same $\Delta\bar{E}^{Rh}_{NP}$. A direct comparison of $\Delta\bar{E}_{NP}$ for each metal under NO and CO environments is shown in Figure S13 of the Supporting Information. NO is observed to stabilize the Rh NP considerably more than CO, while for Pt and Pd the greater particle stabilization due to NO binding is less pronounced. Altogether, these trends, which are manifested by the interplay between coverage dependent adsorption energies, reactant-induced surface stabilization, and NP size, give insight into the variability of particle stability over a broad range of reaction conditions.

**4.4. NP Disintegration Induced by Reactants.** At a specified gas phase chemical potential, the adatom complex that is most likely to form has the most negative disintegration free energy. While a catalytic system is usually not in thermodynamic equilibrium, thermodynamic phase diagrams[81] can function as guidelines for the stability of the system under specific reaction conditions. Therefore, under a given set of operating conditions, one could make predictions about whether the supported NP will be stable against reactant-induced disintegration into adatom complexes, and which species would be most abundant on the support.

*4.4.1. In the Presence of CO.* In previous experiments, Rh and Pt NPs were prepared on $TiO_2(110)$ to be in the range of 10−20 Å with a coverage of $\theta$ = 0.01−0.1 ML, and were subsequently exposed to CO. To make comparisons with these experiments,[23,28] it is assumed that the Rh, Pt, and Pd NPs have particle diameters of 20 Å. Since catalytic applications using supported noble metal NPs typically are well dispersed and are at low particle coverages, and examining disintegration at low particle coverages helps avoid the difficulty of modeling metal-clustering of the adatoms, a surface coverage of $\theta = 0.01$ ML is chosen and the configurational entropy of the adatom complexes is estimated to be $4.83 \times 10^{-4}$ eV/K. The same configurational entropy is assumed for all adatom complexes, and therefore has no influence on the trend variation between Rh, Pt, and Pd. The precise value of the configurational entropy is expected to play a minor part in determining the absolute disintegration free energy compared to the adatom complex formation energy, NP surface energy, and the gas phase chemical potential.

Many experimental studies have reported CO-induced disintegration of Rh NPs on various supports. Scanning tunneling microscope experiments find that the presence of CO can disintegrate Rh NPs on $TiO_2(110)$ of $d$ = 10 to 20 Å near 300 K to form $Rh(CO)_2$ complexes.[23] However, the formation of the $Rh(CO)_2$ complexes was reported to be reversed around 448 K.[23] Likewise, disintegration of $SiO_2$-supported Rh NPs of $d$ = 16 Å into $Rh(CO)_2$ at $10^{-1}$ mbar and 400 K was observed, but under the same conditions Rh NPs of 37 Å were found to be stable against disintegration.[49] CO can also disrupt Rh NPs on $Al_2O_3$, leading to the eventual formation of isolated $Rh(CO)_2$ complexes[26,31,35,36] as well as on MgO between 233 and 300 K.[82] The strong binding of CO to the Rh NPs will weaken the interatomic Rh bonds, and eventually cause formation of the $Rh(CO)_2$ complexes.

CO has been reported to break up Pt crystals into nanosized clusters (which revert to their original morphology after removal of CO)[83] and induce formation of $Pt_x(CO)_x$ complexes on $TiO_2$,[28,41] $ZrO_2$,[84] KL zeolite,[37,38] and MgO(001),[39] indicating that the Pt disintegration phenomena is not extremely sensitive to the support (and similarly for supported Rh NPs as discussed above). Experimentally, 20 Å Pt NPs on $TiO_2(110)$ were observed to undergo CO-induced disintegration into Pt-carbonyl species at 300 K and 0.1 mbar, followed by presumably gas phase Ostwald Ripening due to enhanced diffusion of the weakly bound Pt-carbonyl species.[28] Parkinson et al. has observed mobile Pd(CO) species on $Fe_3O_4(001)$.[22] The authors are unaware of reports involving the disintegration of $Pd/TiO_2$ NPs.

Predictions are made for whether NP disintegration into adatom complexes will occur over a wide range of CO gas phase chemical potentials. In Figure 7, the disintegration free energy for each metal particle is computed to decrease almost linearly with decreases in temperature or increases in pressure. It is predicted that $Rh/TiO_2(110)$ NPs of $d$ = 20 Å would disintegrate into $Rh(CO)_2$ below 318 K at 0.1 mbar under equilibrium conditions ($\Delta G^{dis}_{NP} < 0$), but not at 460 K, in agreement with previous reports.[23,50] Also in accord with past observations and predictions is that Rh(CO) complexes are predicted to not form under these conditions.[23,50]


dx.doi.org/10.1021/jp502201f | J. Phys. Chem. C 2014, 118, 9588−9597

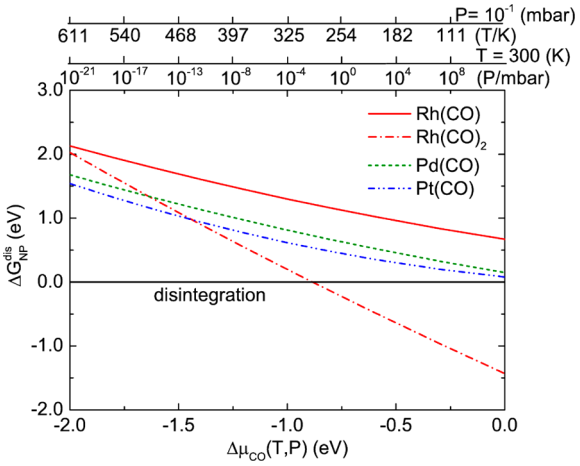


**Figure 7.** Free energy trends for NP disintegration via formation of adatom complexes in the presence of CO. The projected particle diameter is set to 20 Å.

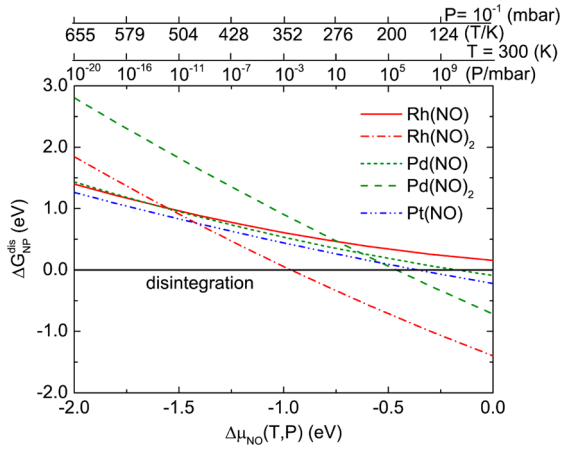


**Figure 8.** Free energy trends for NP disintegration via the formation of adatom complexes in the presence of NO. The projected particle diameter is set to 20 Å.

For $-1.4 < \Delta\mu_{CO} < 0$ eV, Pd NPs are predicted to be the most stable against disintegration for all the metals considered, while Rh NPs are most likely to disintegrate into $Rh(CO)_2$ complexes. Both Pt(CO) and Pd(CO) complexes are computed to have a positive $\Delta G^{dis}_{NP}$ over a broad range of CO chemical potentials. This suggests that the $Pt/TiO_2(110)$ particle disintegration observed in past experiments may instead occur by gas phase species formation, as has been experimentally suggested (and suspected for Pd as well).[28,41] Also, qualitatively, the lower predicted $\Delta G^{dis}_{NP}$ for Rh NPs than for Pt NPs at 300 K and $10^{-1}$ mbar supports experimental observations that $TiO_2(110)$-supported $Rh(CO)_2$ complexes are abundant and more stable against reagglomeration than $Pt(CO)_x$ complexes.[23,28] To achieve redispersion, one must control the reaction conditions and time so the metal adatoms could reagglomerate to form clusters of desired size (however, care must be taken to prevent Ostwald Ripening, which will also depend on reaction conditions, particle coverage, and adatom diffusion barriers).

*4.4.2. In the Presence of NO.* Prior experiments have provided evidence that NO induces the disintegration of 10−20 Å $Rh/TiO_2(110)$ NPs via the formation of isolated $Rh(NO)_2$ at 300 K and 0.1 mbar.[23] Studies of $Pt/TiO_2(110)$ and $Pd/TiO_2(110)$ NPs[25,27] in the presence of NO are less abundant. The $\Delta G^{dis}_{NP}$ for $TiO_2(110)$-supported Rh, Pd, and Pt NPs in the presence of NO is reported in Figure 8. Rh NPs are predicted to favor disintegration into $Rh(NO)_2$ complexes when $\Delta\mu_{NO}$ is less negative than −1.0 eV, and also have the most negative $\Delta G^{dis}_{NP}$ of all the metals considered. Furthermore, Rh NPs are expected to more readily disintegrate in the presence of NO via the formation of $Rh(NO)_2$ complexes compared to $Rh(CO)_2$ (at 300 K the onset of $Rh(NO)_2$ and $Rh(CO)_2$ disintegration would occur near 0.005 mbar NO and 0.008 mbar CO, respectively). In agreement with experimental suggestions, we predict that NO will disintegrate $Rh/TiO_2(110)$ NPs of $d$ = 20 Å into isolated $Rh(NO)_2$ complexes at 300 K and 0.1 mbar.[23] Although Pt NP disintegration into Pt(NO) complexes bound strongly to the support is theoretically possible to occur for a chemical potential above −0.36 eV, in reality this would likely not be experimentally observed due to kinetic hindrances at the required low temperatures (150 K at $10^{-1}$ mbar), or the unreasonably large partial pressures ($\sim 10^5$ mbar at 300 K). Similarly, $Pd(NO)_2$ and Pd(NO) complexes are not predicted to form under typical operating conditions. On the basis of our calculations, it is suspected that the greater Rh adatom stabilization from CO and NO binding compared to the Pd and the Pt adatoms is the key driving force for the facile and stable disintegration of Rh NPs into adatom complexes, while precluding complete disintegration of Pd and Pt NPs under moderate temperatures and pressures.

The effect of varying particle diameter on $\Delta G^{dis}_{NP}$ at 300 K and 0.1 mbar is shown in Figure 9. A rapid decrease in the disintegration free energy is observed for NP diameters less than 25 Å, stemming from the increase of the particle surface area to volume ratio. For each metal, having particle diameters in the range of 10−100 Å, the presence of NO is a stronger promoter of disintegration than CO (except for a predicted crossover at 17 Å for the Rh NP). Under these operating conditions, supported Pd NPs are found to be the most resistant to disintegration compared against Pt and Rh NPs under the same reactive environment.

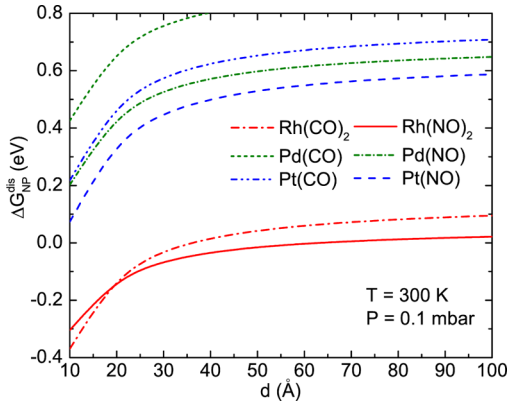


**Figure 9.** Disintegration free energy vs particle diameter in the presence of CO or NO at $T$ = 300 K and $P$ = 0.1 mbar. Only the most favorable adatom complex for each metal is shown.

In qualitative agreement with experiment, $Rh(CO)_2$ complexes are predicted to form from NPs around 35 Å in diameter or less, while $Rh(NO)_2$ complexes are expected to be able to form from NPs of larger sizes ($d$ < 68 Å).[23] This can be rationalized by the more favorable formation energy of the Rh adatom-nitrosyl complexes due to the stronger binding of NO


dx.doi.org/10.1021/jp502201f | J. Phys. Chem. C 2014, 118, 9588−9597

than CO.[85] The disintegration analysis predicts that Pd and Pt NPs are stable toward complete disintegration into isolated and strongly bound adatom-carbonyl complexes between 10 and 100 Å at 300 K and 0.1 mbar. Indeed, these species typically cannot be experimentally detected,[41] although the Rh and Ir counterparts are readily observed. Interestingly, the addition of NO has been reported to enhance the formation of $Rh(CO)_2$ complexes,[82] which was attributed to weakening of Rh−Rh interatomic bonds—thus future work could entail considering the mixing of gas species in the disintegration analysis.

Besides NP disintegration via the formation of adatom complexes on the support, it should be reemphasized that gas phase disintegration, for instance via the formation of volatile oxides in the presence of oxygen, can occur.[9,29,67−69] A more complete picture of NP disintegration, and even sintering, in the presence of reactants should include the role of volatile metal−reactant species. Including vapor disintegration and looking at support effects on NP disintegration are directions for future research.

## 5. CONCLUSIONS

Understanding supported transition metal catalysts is imperative since they are used in a vast array of environmentally and industrially important processes such as the reduction of toxic gases like $NO_x$ and CO. In this study, ab initio atomistic thermodynamics were used to gain an understanding of the effects of NO and CO on the stability of precious three-way catalysts, namely, Rh, Pt, and Pd NPs supported on $TiO_2(110)$, under realistic temperatures and pressures.

Following a recent methodology developed by Ouyang et al.,[50] the influence of NO and CO adsorption on Rh, Pt, and Pd NP energetics and stability toward disintegration into adatom complexes was investigated under a variety of system conditions, i.e., particle size, temperature, and pressure. Computed formation energies of metal adatoms and adatom complexes were presented, and Rh adatom complexes were predicted to be generally more stable than Pd or Pt adatom complexes. The NO and CO chemical potential and particle size influences on NP stability were explored, and supported Rh NP stability toward disintegration was found to be more sensitive to the presence of either CO or NO than supported Pt or Pd NPs. In agreement with experiments, predictions are made that either CO and NO can cause $Rh/TiO_2(110)$ to disintegrate at 300 K and 0.1 mbar via formation of dicarbonyl or dinitrosyl adatom complexes. $TiO_2(110)$-supported Pt or Pd NPs behave similarly, and both are more resistant to CO- and NO-induced disintegration than supported Rh NPs.

Over a broad range of reaction conditions NO was found to be a more efficient reactant for particle disintegration and/or redispersion than CO. Compared to Pd and Pt, Rh is more susceptible to reactant-induced disintegration, due to the large and exothermic formation energy of Rh adatom complexes. To prevent the disintegration of three-way catalysts induced by CO and NO, further investigations of the Rh−support interaction, Rh particle size distribution, as well as the reaction conditions limiting the formation of the Rh−nitrosyl and Rh−carbonyl complexes are required. The insights revealed are expected to be valuable for either preventing catalyst deactivation due to reactant-induced NP disintegration or facilitating reactant-induced redispersion of sintered catalysts.

## ■ ASSOCIATED CONTENT

### Supporting Information

Figures containing computed adatom and adatom complex adsorption positions, average binding energies as a function of surface coverage, and free energy trends for NP disintegration via the formation of adatom complexes. This material is available free of charge via the Internet at http://pubs.acs.org.

## ■ AUTHOR INFORMATION

### Corresponding Author

*E-mail: wxli@dicp.ac.cn. Tel: 0086-411-84379996. Fax: 0086-411-84694447.

### Notes

The authors declare no competing financial interest.

## ■ ACKNOWLEDGMENTS

This work was funded by the NSFC (21173210, 21225315), the 973 Program (2013CB834603), the NSF-OISE 0530268, and the CAS (XDA09030101). B.R.G. acknowledges the PIRE-ECCI program for a graduate fellowship. E.D.S. thanks IRES-ECCI for an undergraduate summer research fellowship. We thank Jin-Xun Liu for providing a script to facilitate Wulff construction of nanoparticles and Saswata Bhattacharya for providing helpful suggestions.

## ■ REFERENCES

(1) Farrauto, R. J.; Heck, R. M. Catalytic Converters: State of the Art and Perspectives. *Catal. Today* **1999**, *51*, 351−360.
(2) Shelef, M.; McCabe, R. W. Twenty-five Years After Introduction of Automotive Catalysts: What Next? *Catal. Today* **2000**, *62*, 35−50.
(3) Kašpar, J.; Fornasiero, P.; Hickey, N. Automotive Catalytic Converters: Current Status and Some Perspectives. *Catal. Today* **2003**, *77*, 419−449.
(4) Valden, M.; Lai, X.; Goodman, D. W. Onset of Catalytic Activity of Gold Clusters on Titania with the Appearance of Nonmetallic Properties. *Science* **1998**, *281*, 1647−1650.
(5) Feldheim, D. L.; Foss, C. A. J. *Metal Nanoparticles: Synthesis, Characterization, and Applications*; Marcel Dekker Incorporated: New York, NY, 2002.
(6) Haruta, M. When Gold Is Not Noble: Catalysis by Nanoparticles. *Chem. Rec.* **2003**, *3*, 75−87.
(7) Cao, G. Z.; Wang, Y. *Nanostructures and Nanomaterials: Synthesis, Properties, and Applications*; World Scientific Publishing Company Incorporated: Singapore, Singapore, 2011.
(8) Bartholomew, C. H. Sintering and Redispersion of Supported Metals: Perspectives from the Literature of the Past Decade. In *Studies in Surface Science and Catalysis*; Bartholomew, C. H., Fuentes, G. A., Eds.; Elsevier: New York, NY, 1997; Vol. *111*; pp 585−592.
(9) Bartholomew, C. H. Mechanisms of Catalyst Deactivation. *Appl. Catal., A* **2001**, *212*, 17−60.
(10) Schmid, G. *Nanoparticles: From Theory to Application*; Wiley: New York, NY, 2004.
(11) Moshfegh, A. Z. Nanoparticle Catalysts. *J. Phys. D: Appl. Phys.* **2009**, *42*, 233001.
(12) Bowker, M.; James, D.; Stone, P.; Bennett, R.; Perkins, N.; Millard, L.; Greaves, J.; Dickinson, A. Catalysis at the Metal-Support Interface: Exemplified by the Photocatalytic Reforming of Methanol on $Pd/TiO_2$. *J. Catal.* **2003**, *217*, 427−433.
(13) Qiang, F.; Li, W.-X.; Yao, Y.; Liu, H.; Su, H.-Y.; Ma, D.; Gu, X.-K.; Chen, L.; Wang, Z.; Zhang, H.; et al. Interface-Confined Ferrous Centers for Catalytic Oxidation. *Science* **2010**, *328*, 1141−1144.
(14) Cargnello, M.; Doan-Nguyen, V. V. T.; Gordon, T. R.; Diaz, R. E.; Stach, E. A.; Gorte, R. J.; Fornasiero, P.; Murray, C. B. Control of Metal Nanocrystal Size Reveals Metal-Support Interface Role for Ceria Catalysts. *Science* **2013**, *341*, 771−773.

(15) Daniel, M.-C.; Astruc, D. Gold Nanoparticles: Assembly, Supramolecular Chemistry, Quantum-Size-Related Properties, and Applications Toward Biology, Catalysis, and Nanotechnology. *Chem. Rev.* **2004**, *104*, 293−346.
(16) Lopez-Acevedo, O.; Kacprzak, K. A.; Akola, J.; Häkkinen, H. Quantum Size Effects in Ambient CO Oxidation Catalysed by Ligand-Protected Gold Clusters. *Nat. Chem.* **2010**, *2*, 329−334.
(17) Wanke, S. Sintering and Redispersion of Conventional Supported Metal Catalysts in Hydrogen and Oxygen Atmospheres. In *Materials Science Research*; Kuczynski, G., Miller, A., Sargent, G., Eds.; Springer: Secaucus, NJ, 1984; pp 223−242.
(18) Harris, P. J. F. Growth and Structure of Supported Metal Catalyst Particles. *Int. Mater. Rev.* **1995**, *40*, 97−115.
(19) Sehested, J.; Gelten, J. A. P.; Remediakis, I. N.; Bengaard, H.; Nørskov, J. K. Sintering of Nickel Steam-Reforming Catalysts: Effects of Temperature and Steam and Hydrogen Pressures. *J. Catal.* **2004**, *223*, 432−443.
(20) Simonsen, S. B.; Chorkendorff, I.; Dahl, S.; Skoglundh, M.; Sehested, J.; Helveg, S. Direct Observations of Oxygen-induced Platinum Nanoparticle Ripening Studied by In Situ TEM. *J. Am. Chem. Soc.* **2010**, *132*, 7968−7975.
(21) Nagai, Y.; Dohmae, K.; Ikeda, Y.; Takagi, N.; Hara, N.; Tanabe, T.; Guilera, G.; Pascarelli, S.; Newton, M. A.; Takahashi, N.; et al. In Situ Observation of Platinum Sintering on Ceria-Based Oxide for Autoexhaust Catalysts using Turbo-XAS. *Catal. Today* **2011**, *175*, 133−140.
(22) Parkinson, G. S.; Novotny, Z.; Argentero, G.; Schmid, M.; Pavelec, J.; Kosak, R.; Blaha, P.; Diebold, U. Carbon Monoxide-Induced Adatom Sintering in a Pd-$Fe_3O_4$ Model Catalyst. *Nat. Mater.* **2013**, *12*, 724−728.
(23) Berkó, A.; Solymosi, F. Adsorption-Induced Structural Changes of Rh Supported by $TiO_2$(110)-(1 × 2): An STM Study. *J. Catal.* **1999**, *183*, 91−101.
(24) Starr, D.; Shaikhutdinov, S.; Freund, H.-J. Gold Supported on Oxide Surfaces: Environmental Effects as Studied by STM. *Top. Catal.* **2005**, *36*, 33−41.
(25) Newton, M. A.; Belver-Coldeira, C.; Martínez-Arias, A.; Fernández-García, M. Dynamic In Situ Observation of Rapid Size and Shape Change of Supported Pd Nanoparticles during CO/NO Cycling. *Nat. Mater.* **2007**, *6*, 528−533.
(26) Dent, A. J.; Evans, J.; Fiddy, S. G.; Jyoti, B.; Newton, M. A.; Tromp, M. Rhodium Dispersion during NO/CO Conversions. *Angew. Chem., Int. Ed* **2007**, *46*, 5356−5358.
(27) Newton, M. A.; Belver-Coldeira, C.; Martínez-Arias, A.; Fernández-García, M. "Oxidationless" Promotion of Rapid Palladium Redispersion by Oxygen during Redox CO/(NO+$O_2$) Cycling. *Angew. Chem.* **2007**, *119*, 8783−8785.
(28) Berkó, A.; Szökő, J.; Solymosi, F. Effect of CO on the Morphology of Pt Nanoparticles Supported on $TiO_2$(110)-(1×*n*). *Surf. Sci.* **2004**, *566*, 337−342.
(29) Porsgaard, S.; Merte, L. R.; Ono, L. K.; Behafarid, F.; Matos, J.; Helveg, S.; Salmeron, M.; Roldan Cuenya, B.; Besenbacher, F. Stability of Platinum Nanoparticles Supported on $SiO_2$/Si(111): A High-Pressure X-ray Photoelectron Spectroscopy Study. *ACS Nano* **2012**, *6*, 10743−10749.
(30) Ratke, L.; Voorhees, P. W. *Growth and Coarsening: Ostwald Ripening in Material Processing*; Springer: Secaucus, NJ, 2002.
(31) Solymosi, F.; Pásztor, M. An Infrared Study of the Influence of CO Chemisorption on the Topology of Supported Rhodium. *J. Phys. Chem.* **1985**, *89*, 4789−4793.
(32) Mizushima, T.; Tohji, K.; Udagawa, Y.; Ueno, A. EXAFS Study of the Carbon Monoxide Adsorption-Induced Morphology Change in Ruthenium Clusters Supported on Alumina. *J. Phys. Chem.* **1990**, *94*, 4980−4985.
(33) Horch, S.; Lorensen, H. T.; Helveg, S.; Lægsgaard, E.; Stensgaard, I.; Jacobsen, K. W.; Nørskov, J. K.; Besenbacher, F. Enhancement of Surface Self-Diffusion of Platinum Atoms by Adsorbed Hydrogen. *Nature* **1999**, *398*, 134−136.
(34) Gerber, T.; Knudsen, J.; Feibelman, P. J.; Grånäs, E.; Stratmann, P.; Schulte, K.; Andersen, J. N.; Michely, T. CO-Induced Smoluchowski Ripening of Pt Cluster Arrays on the Graphene/Ir(111) Moiré. *ACS Nano* **2013**, *7*, 2020−2031.
(35) van't Blik, H. F. J.; van Zon, J. B. A. D.; Huizinga, T.; Vis, J. C.; Koningsberger, D. C.; Prins, R. Structure of Rhodium in an Ultradispersed Rhodium/Alumina Catalyst as Studied by EXAFS and Other Techniques. *J. Am. Chem. Soc.* **1985**, *107*, 3139−3147.
(36) Solymosi, F.; Pásztor, M. Infrared Study of the Effect of $H_2$ on CO-Induced Structural Changes in Supported Rh. *J. Phys. Chem.* **1986**, *90*, 5312−5317.
(37) Vicente, B. C.; Nelson, R. C.; Singh, J.; Scott, S. L.; van Bokhoven, J. A. Electronic Structures of Supported Pt and PtSn Nanoparticles in the Presence of Adsorbates and during CO Oxidation. *Catal. Today* **2011**, *160*, 137−143.
(38) Stakheev, A. Y.; Shpiro, E. S.; Jaeger, N. I.; Schulz-Ekloff, G. FTIR Evidence of the Formation of Platinum Carbonyls from Pt Metal Clusters Encaged in KL Zeolite. *Catal. Lett.* **1995**, *34*, 293−303.
(39) Chaâbane, N.; Lazzari, R.; Jupille, J.; Renaud, G.; Avellar Soares, E. CO-Induced Scavenging of Supported Pt Nanoclusters: A GISAXS Study. *J. Phys. Chem. C* **2012**, *116*, 23362−23370.
(40) Akdogan, Y.; Anantharaman, S.; Liu, X.; Lahiri, G. K.; Bertagnolli, H.; Roduner, E. Reconstruction of $Pt_{13}$ Clusters into $Pt_2(CO)_m$ on CO Addition in NaY Zeolite. *J. Phys. Chem. C* **2009**, *113*, 2352−2359.
(41) Raskó, J. CO-Induced Surface Structural Changes of Pt on Oxide-Supported Pt Catalysts Studied by DRIFTS. *J. Catal.* **2003**, *217*, 478−486.
(42) Solymosi, F.; Novak, E.; Molnar, A. Infrared Spectroscopic Study on Carbon Monoxide-Induced Structural Changes of Iridium on an Alumina Support. *J. Phys. Chem.* **1990**, *94*, 7250−7255.
(43) Gupta, N.; Londhe, V.; Kamble, V. Gas-Uptake, Methanation, and Microcalorimetric Measurements on the Coadsorption of CO and $H_2$ over Polycrystalline Ru and a Ru/$TiO_2$ Catalyst. *J. Catal.* **1997**, *169*, 423−437.
(44) Sá, J.; Taylor, S. F. R.; Daly, H.; Goguet, A.; Tiruvalam, R.; He, Q.; Kiely, C. J.; Hutchings, G. J.; Hardacre, C. Redispersion of Gold Supported on Oxides. *ACS Catal.* **2012**, *2*, 552−560.
(45) Banerjee, A.; Theron, R.; Scott, R. W. J. Redispersion of Transition Metal Nanoparticle Catalysts in Tetraalkylphosphonium Ionic Liquids. *Chem. Commun.* **2013**, *49*, 3227−3229.
(46) Galisteo, F. C.; Mariscal, R.; Granados, M. L.; Fierro, J.; Daley, R.; Anderson, J. Reactivation of Sintered Pt/$Al_2O_3$ Oxidation Catalysts. *Appl. Catal., B* **2005**, *59*, 227−233.
(47) Birgersson, H.; Eriksson, L.; Boutonnet, M.; Järås, S. G. Thermal Gas Treatment to Regenerate Spent Automotive Three-Way Exhaust Gas Catalysts (TWC). *Appl. Catal., B* **2004**, *54*, 193−200.
(48) Goguet, A.; Hardacre, C.; Harvey, I.; Narasimharao, K.; Saih, Y.; Sa, J. Increased Dispersion of Supported Gold during Methanol Carbonylation Conditions. *J. Am. Chem. Soc.* **2009**, *131*, 6973−6975.
(49) McClure, S. M.; Lundwall, M. J.; Goodman, D. W. Planar Oxide Supported Rhodium Nanoparticles as Model Catalysts. *Proc. Natl. Acad. Sci. U.S.A.* **2011**, *108*, 931−936.
(50) Ouyang, R.; Liu, J.-X.; Li, W.-X. Atomistic Theory of Ostwald Ripening and Disintegration of Supported Metal Particles under Reaction Conditions. *J. Am. Chem. Soc.* **2013**, *135*, 1760−1771.
(51) Reuter, K.; Scheffler, M. Composition, Structure, and Stability of $RuO_2$(110) as a Function of Oxygen Pressure. *Phys. Rev. B* **2001**, *65*, 035406.
(52) Li, W.-X.; Stampfl, C.; Scheffler, M. Why is a Noble Metal Catalytically Active? The Role of the O-Ag Interaction in the Function of Silver as an Oxidation Catalyst. *Phys. Rev. Lett.* **2003**, *90*, 256102.
(53) Li, W.-X.; Stampfl, C.; Scheffler, M. Insights into the Function of Silver as an Oxidation Catalyst by *Ab Initio* Atomistic Thermodynamics. *Phys. Rev. B* **2003**, *68*, 165412.
(54) Reuter, K.; Stampf, C.; Scheffler, M. Ab Initio Atomistic Thermodynamics and Statistical Mechanics of Surface Properties and Functions. In *Handbook of Materials Modeling*; Yip, S., Ed.; Springer: Dordrecht, The Netherlands, 2005; pp 149−194.

(55) Kresse, G.; Hafner, J. Ab Initio Molecular Dynamics for Liquid Metals. *Phys. Rev. B* **1993**, *47*, 558−562.
(56) Kresse, G.; Furthmüller, J. Efficiency of Ab-Initio Total Energy Calculations for Metals and Semiconductors using a Plane-Wave Basis Set. *Comput. Mater. Sci.* **1996**, *6*, 15−50.
(57) Kresse, G.; Furthmüller, J. Efficient Iterative Schemes for Ab Initio Total-Energy Calculations using a Plane-Wave Basis Set. *Phys. Rev. B* **1996**, *54*, 11169−11186.
(58) Blöchl, P. E. Projector Augmented-wave Method. *Phys. Rev. B* **1994**, *50*, 17953−17979.
(59) Hammer, B.; Hansen, L. B.; Nørskov, J. K. Improved Adsorption Energetics within Density-Functional Theory using Revised Perdew-Burke-Ernzerhof Functionals. *Phys. Rev. B* **1999**, *59*, 7413−7421.
(60) Thompson, S. J.; Lewis, S. P. Revisiting the (110) Surface Structure of $TiO_2$: A Theoretical Analysis. *Phys. Rev. B* **2006**, *73*, 73403.
(61) Feynman, R. P. Forces in Molecules. *Phys. Rev.* **1939**, *56*, 340−343.
(62) Chrétien, S.; Metiu, H. Density Functional Study of the Interaction Between Small Au Clusters, $Au_n$ (n = 1−7) and the Rutile $TiO_2$ Surface. I. Adsorption on the Stoichiometric Surface. *J. Chem. Phys.* **2007**, *127*, 244708.
(63) Kim, H. Y.; Lee, H. M.; Pala, R. G. S.; Shapovalov, V.; Metiu, H. CO Oxidation by Rutile $TiO_2$(110) Doped with V, W, Cr, Mo, and Mn. *J. Phys. Chem. C* **2008**, *112*, 12398−12408.
(64) Singh-Miller, N. E.; Marzari, N. Surface Energies, Work Functions, and Surface Relaxations of Low-Index Metallic Surfaces from First Principles. *Phys. Rev. B* **2009**, *80*, 235407.
(65) Kittel, C. *Introduction to Solid State Physics*; John Wiley & Sons: Hoboken, NJ, 1956.
(66) Bredow, T.; Pacchioni, G. A Quantum-Chemical Study of Pd Atoms and Dimers Supported on $TiO_2$(110) and their Interaction with CO. *Surf. Sci.* **1999**, *426*, 106−122.
(67) Schäfer, H.; Tebben, A. Gleichgewichtsmessungen im System Platin-Sauerstoff. *Anorg. Chem.* **1960**, *304*, 317−321.
(68) Chaston, J. C. The Oxidation of the Platinum Metals. *Platinum Met. Rev.* **1975**, *19*, 135−140.
(69) Alcock, C. B.; Hooper, G. W. Thermodynamics of the Gaseous Oxides of the Platinum-Group Metals. *Proc. R. Soc. London, Ser. A* **1960**, *254*, 551−561.
(70) Vitos, L.; Ruban, A. V.; Skriver, H. L.; Kollár, J. The Surface Energy of Metals. *Surf. Sci.* **1998**, *411*, 186−202.
(71) Bowker, M.; Stone, P.; Bennett, R.; Perkins, N. CO Adsorption on a Pd/$TiO_2$(110) Model Catalyst. *Surf. Sci.* **2002**, *497*, 155−165.
(72) Yudanov, I. V.; Genest, A.; Schauermann, S.; Freund, H.-J.; Rösch, N. Size Dependence of the Adsorption Energy of CO on Metal Nanoparticles: A DFT Search for the Minimum Value. *Nano Lett.* **2012**, *12*, 2134−2139.
(73) Campbell, C. T.; Parker, S. C.; Starr, D. E. The Effect of Size-Dependent Nanoparticle Energetics on Catalyst Sintering. *Science* **2002**, *298*, 811−814.
(74) Chen, R.; Chen, Z.; Ma, B.; Hao, X.; Kapur, N.; Hyun, J.; Cho, K.; Shan, B. CO Adsorption on Pt (111) and Pd (111) Surfaces: A First-Principles Based Lattice Gas Monte-Carlo Study. *Comput. Theor. Chem.* **2012**, *987*, 77−83.
(75) Zeng, Z.-H.; Da Silva, J. L. F.; Li, W.-X. Theory of Nitride Oxide Adsorption on Transition Metal (111) Surfaces: a First-Principles Investigation. *Phys. Chem. Chem. Phys.* **2010**, *12*, 2459−2470.
(76) Sautet, P.; Rose, M. K.; Dunphy, J. C.; Behler, S.; Salmeron, M. Adsorption and Energetics of Isolated CO Molecules on Pd(111). *Surf. Sci.* **2000**, *453*, 25−31.
(77) Nakamura, I.; Fujitani, T.; Hamada, H. Adsorption and Decomposition of NO on Pd Surfaces. *Surf. Sci.* **2002**, *514*, 409−413.
(78) Getman, R. B.; Schneider, W. F. DFT-Based Characterization of the Multiple Adsorption Modes of Nitrogen Oxides on Pt(111). *J. Chem. Phys. C* **2006**, *111*, 389−397.
(79) Chase, J. M. W.; Davies, C. A.; Davies, J. R.; Fulrip, D. J.; McDonald, R. A.; Syverud, A. N. JANAF Thermodynamic Tables. *J. Phys. Chem. Ref. Data* **1985**, *14*.
(80) Barmparis, G. D.; Remediakis, I. N. Dependence on CO Adsorption of the Shapes of Multifaceted Gold Nanoparticles: A Density Functional Theory. *Phys. Rev. B* **2012**, *86*, 085457.
(81) Bhattacharya, S.; Levchenko, S. V.; Ghiringhelli, L. M.; Scheffler, M. Stability and Metastability of Clusters in a Reactive Atmosphere: Theoretical Evidence for Unexpected Stoichiometries of $Mg_mO_x$. *Phys. Rev. Lett.* **2013**, *111*, 135501.
(82) Novák, E.; Sprinceana, D.; Solymosi, F. CO-Induced Structural Changes of Supported Rh promoted by NO. *Appl. Catal., A* **1997**, *149*, 89−101.
(83) Tao, F.; Dag, S.; Wang, L.-W.; Liu, Z.; Butcher, D. R.; Bluhm, H.; Salmeron, M.; Somorjai, G. A. Break-Up of Stepped Platinum Catalyst Surfaces by High CO Coverage. *Science* **2010**, *327*, 850−853.
(84) Benvenutti, E. V.; Franken, L.; Moro, C. C.; Davanzo, C. U. FTIR Study of Hydrogen and Carbon Monoxide Adsorption on Pt/$TiO_2$, Pt/$ZrO_2$, and Pt/$Al_2O_3$. *Langmuir* **1999**, *15*, 8140−8146.
(85) Zhdanov, V. P.; Kasemo, B. Mechanism and Kinetics of the NO-CO Reaction on Rh. *Surf. Sci. Rep.* **1997**, *29*, 31−90.